Available online at www.sciencedirect.com
ScienceDirect
Journal of Catalysis 247 (2007) 155–165
JOURNAL OF CATALYSIS
www.elsevier.com/locate/jcat

Design of catalyst systems for the one-pot synthesis of menthols from citral

A.F. Trasarti, A.J. Marchi, C.R. Apesteguía *

Catalysis Science and Engineering Research Group (GICIC), Instituto de Investigaciones en Catálisis y Petroquímica–INCAPE (UNL-CONICET), Santiago del Estero 2654, (3000) Santa Fe, Argentina

Received 8 November 2006; revised 28 December 2006; accepted 28 January 2007

Available online 7 March 2007

Abstract

Stable, active, and highly selective bifunctional Ni/Al-MCM-41 catalysts were developed for the one-pot synthesis of menthols from citral. The liquid-phase hydrogenation of citral to citronellal was studied on silica-supported noble (Pt, Pd, Ir) and nonnoble (Ni, Co, Cu) metals. It was found that citronellal is selectively formed at the beginning of the reaction only on Pd and Ni catalysts. The consecutive ene-cyclization of citronellal to isopulegols was investigated on solid acids containing exclusively Lewis (ZnO/SiO_2) or strong Brönsted (CsHPA) acid sites, and also on catalysts containing both Lewis and Brönsted acid sites of either strong (zeolites, SiO_2–Al_2O_3) or moderate (Al-MCM-41) strength. The isopulegol formation rate was higher on samples exhibiting dual Lewis/Brönsted acidity, such as SiO_2–Al_2O_3, Al-MCM-41, and zeolite HBEA. Based on these previous results, bifunctional catalysts containing Pd or Ni supported on SiO_2–Al_2O_3, Al-MCM-41, or zeolite HBEA were prepared and tested for citral conversion to menthols. The catalyst stability and the effect of hydrogen pressure and metal loading on menthol productivity were also investigated. The best catalyst was Ni(8%)/Al-MCM-41, which yielded more than 90% menthols at 2026.0 kPa and showed no significant deactivation after two consecutive catalytic tests.

Keywords: Menthol synthesis; Citral; Selective hydrogenation; Ni catalysts; Citronellal; Isopulegols; Metal/acid catalysts

1. Introduction

Menthol has the largest world demand among the mint products, being widely used in pharmaceuticals and toothpastes, with secondary applications in chewing gum, cigarettes, and confectionery. Of the four pairs of optical menthol isomers—(±)-menthol, (±)-isomenthol, (±)-neomenthol, and (±)-neoisomenthol—only (−)-menthol has the characteristic peppermint odor and exerts a unique cooling sensation on the skin and mucous membranes. The racemic (±)-menthol mixture has also industrial applications, although its refreshing effect is lower than that of (−)-menthol. The world market for (−)-menthol comprises natural (80%) and synthetic (20%) materials, and total demand is in the order of 12,000 tons/year [1]. Natural menthol is obtained mainly by separation of *Mentha* piperita essential oil, whereas synthetic menthol is produced by two companies, Harrmann & Reimer and Takasago International Corp. The Harrmann & Reimer process [2,3] is the first commercial synthetic route to (−)-menthol. In this process, thymol is first obtained by propylation of *m*-cresol and then hydrogenated to racemic (±)-menthols; (−)-menthol is obtained by further treating the racemic menthol via a separation crystallization process. The Takasago process produces (−)-menthol from myrcene using a chiral Rh BINAP catalyst for transforming diethylgeranylamine obtained from myrcene to the chiral 3R-citronelal enamine with >95% enantiomeric excess [4,5].

Considerable effort has been devoted to the production of menthols by synthetic or semisynthetic means from other, more readily reliable raw materials. We recently reported for the first time the one-pot synthesis of menthols from citral [6]. Citral (3,7-dimethyl-2,6-octadien-1-al) is a widely used key building block in fine chemicals, particularly in the production of vitamins A and E, as well as carotenoids and an extended range of aroma chemicals [7]. The worldwide demand for citral has increased significantly in recent years due to the increasing need for high-quality products in animal nutrition, food production, and innovative cosmetics. Consequently, fine chemistry companies have invested in citral and its derivatives to expand the

* Corresponding author. Fax: +54 342 4531068.
E-mail address: capesteg@fiqus.unl.edu.ar (C.R. Apesteguía).

0021-9517/$ – see front matter
doi:10.1016/j.jcat.2007.01.016

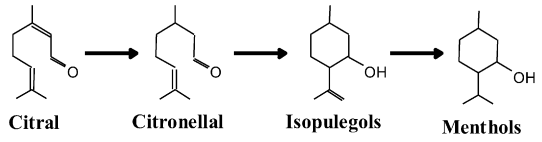

Scheme 1. Reaction sequence for menthol synthesis from citral.

production scale and meet market demand. For example, in 2004 BASF inaugurated a world-scale plant in Ludwigshafen, Germany, with an annual capacity of 40,000 metric tons, replacing an existing plant with a capacity of 10,000 metric tons/year. This new citral production plant uses a more ecologically and economically favorable process that starts with cheaply available isobutene and formaldehyde [8]. Citral is also a renewable raw material that may be obtained by distillation of essential oils, such as lemongrass oil, which contains ca. 70–80% citral. The selective synthesis of menthols from citral in a one-step process involves the initial hydrogenation of citral to citronellal, followed by the isomerization of citronellal to isopulegols and the final hydrogenation of isopulegols to menthols [6], as depicted in Scheme 1.

The consecutive reactions involved in the citral-to-menthols pathway of Scheme 1 have been studied separately, but often the objectives of these studies were not directed to the synthesis of menthols. For example, the selective hydrogenation of citral has been widely investigated on different metal-supported catalysts for producing either nerol/geraniol [9–13] or citronellol [14–17]; few papers have dealt specifically with the selective hydrogenation of citral to citronellal [18–20]. The second reaction in the sequence of Scheme 1 is the conversion of citronellal to isopulegols. The citronellal molecule has two prochiral carbon atoms that generate asymmetrical centers in isopulegol; there actually are four pairs of enantiomers of isopulegols, but only (−)-isopulegol is selectively hydrogenated to (−)-menthol. In the Takasago process, the intramolecular ene-cyclization of (+)-citronellal to (−)-isopulegol is efficiently carried out using large quantities of aqueous $ZnBr_2$. A number of papers have specifically studied the transformation of (+)-citronellal to (−)-isopulegol by using Lewis acids or molybdenum and tungsten complexes as homogeneous catalysts [21–23]. However, these homogeneous processes entail concerns related to toxicity, catalyst reuse, and disposal of spent acid materials. Thus, increasing efforts have been devoted to developing active and recyclable solid acids for obtaining isopulegols from citronellal. Acid zeolites, such as zeolites HY, MCM-22, and HBEA, as well as supported heteropoly acid $H_3PW_{12}O_{40}$, sulfated zirconia, and zirconium hydroxide, have been studied in the citronellal conversion reaction [24–27]. Finally, the direct synthesis of citronellal to menthol was investigated on Ru- [28], Cu- [29], and Pt-supported catalysts [30].

We reported for the first time in a research note [6] the highly selective synthesis of menthols from citral in a one-step process using bifunctional metal/acid catalysts. Conclusions of this work were recently confirmed by other authors [31]. In this paper, we present a detailed study on the development of active, selective, and stable bifunctional catalysts for the one-pot synthesis of menthols from citral. We first investigated the liquid-phase hydrogenation of citral to citronellal on silica-supported noble (Pt, Pd, Ir) and nonnoble (Ni, Co, Cu) metals to select those metals exhibiting the highest initial formation rates of citronellal. Then we studied the isomerization of citronellal to isopolulegols on solid acids containing only Lewis (ZnO/SiO_2) or strong Brönsted (CsHPA) acid sites, and also on catalysts containing both Lewis and Brönsted acid sites of either strong (zeolites, $Si_2–Al_2O_3$) or moderate (Al-MCM-41) strength. The objective was to ascertain the requirements of surface acid site density and strength to promote the ene-cyclization of citronellal to isopolulegols. Based on these catalytic results, we finally prepared bifunctional metal/acid catalysts that were tested in the conversion of citral. We also investigated the effect of changing hydrogen pressure and the metal loading on the menthol formation rate. Finally, we performed consecutive catalytic tests to establish the catalyst stability during reaction. Results will show that at 2026.0 kPa total pressure, the Ni(8%)/Al-MCM-41 sample yields more than 90% menthols from citral and gives 70–75% of racemic (±)-menthol into the menthol mixture without presenting any noticeable activity decay after performing two consecutive catalytic tests.

2. Experimental

2.1. Catalyst preparation

The H form of zeolite HZSM5 was prepared by triple ion exchange of a commercial NaZSM5 zeolite (Zeocat Pentasil PZ-2/54) with ammonium acetate (Sigma, 99%) at 298 K and subsequent calcination in air. $ZnO(25\%)/SiO_2$ was made by incipient-wetness impregnation at 303 K of Grace G62 SiO_2 with an aqueous solution of $ZnCl_2$ (Riedel de Haën, 98.5%). After impregnation, the sample was dried overnight at 363 K and then treated in air at 673 K for 2 h. $SiO_2–Al_2O_3$ (Aldrich, 135 grade) and commercial zeolite HBEA (Zeocat PB) were calcined in air at 773 K for 4 h. CsHPA ($Cs_{2.5}H_{0.5}PW_{12}O_{40}$) was obtained by precipitation, by adding a solution of Cs_2CO_3 (Sigma) dropwise to an aqueous solution of $H_3PW_{12}O_{40}·6H_2O$ (HPA, Merck p.a.). The precipitate was filtered and dried overnight at 363 K, then calcined in air at 573 for 4 h. Al-MCM-41 (Si/Al = 10) was synthesized according to Edler and White [32]. Sodium silicate solution (14% NaOH and 27% SiO_2, Aldrich), cetyltrimethylammonium bromide (Aldrich), aluminum isopropoxide, and deionized water were used as reagents. The composition of the synthesis gel was $7SiO_2–xAl_2O_3–2.7Na_2O–3.7CTMABr–1000H_2O$. The pH was adjusted to 10 using a 1 M H_2SO_4 solution, after which the gel was transferred to a Teflon-lined stainless-steel autoclave and heated to 373 K in an oven for 96 h. After crystallization, the solid was washed with deionized water, dried at 373 K, and finally calcined at 773 K for 4 h.

Silica-supported catalysts were prepared by supporting Pt, Pd, Ir, Ni, Co, or Cu on a SiO_2 powder (Grace G62, 99.7%). The silica had a BET surface area (S_g) of 230 m^2/g and a pore volume of 1.19 cm^3/g. Metal nitrate solutions were used for impregnating Pd, Co, Ni, and Cu, and Ir/SiO_2 was prepared using an H_2IrCl_6 precursor. Pt/SiO_2 catalyst was created by incipient-

wetness impregnation at 303 K with a 0.007 M aqueous solution of tetraamine platinum nitrate, $Pt(NH_3)_4(NO_3)_2$ (Alfa). The impregnated silica was dried overnight at 363 K, then heated in nitrogen at 5 K/min to 673 K and kept at this temperature for 2 h. The other metal/SiO_2 catalysts were prepared following the same preparation procedure as for Pt/SiO_2, but the calcination at 673 K was performed in air instead of nitrogen.

Nickel supported on zeolite HBEA (Ni/HBEA), Al-MCM-41 (Ni/Al-MCM-41), and silica–alumina (Ni/SiO_2–Al_2O_3) were obtained by incipient-wetness impregnation at 303 K, using $Ni(NO_3)_2$ (Alfa) aqueous solutions of 0.25, 0.14, and 0.32 M, respectively. The impregnated samples were dried overnight at 363 K, treated in air at 673 K for 6 h, and finally reduced in H_2 for 2 h at 723 K. Sample Pd/HBEA was prepared by impregnating the Zeocat HBEA zeolite with a 0.05 M aqueous solution of $Pd(NO_3)_2$. After drying overnight at 363 K, the sample was heated in air from room temperature up to 773 K at 1 K/min and then kept at this temperature for 4 h.

2.2. Catalyst characterization

The temperature-programmed reduction (TPR) experiments were performed in a Okhura TPD 20025 unit, using a 5% H_2/Ar gaseous mixture at 60 cm^3/min STP. The sample size was 150 mg. Samples were heated from 298 to 1073 K at 10 K/min. Because water was formed during sample reduction, the gas exiting from the reactor was passed through a cold trap before entering the thermal conductivity detector.

Acid site densities were determined by temperature-programmed desorption (TPD) of NH_3 preadsorbed at 373 K. Samples (0.200 g) were treated in He (60 ml/min) at 773 K for 0.5 h and then exposed to a 1% NH_3/He stream for 40 min at 373 K. Weakly adsorbed NH_3 was removed by flowing He at 373 K during 2 h. Temperature was then increased at a rate of 10 K/min, and the NH_3 concentration in the effluent was measured by mass spectrometry (MS) in a Baltzers Omnistar unit.

The nature of surface acid sites was determined by Fourier transform infrared spectroscopy (FTIR), using pyridine as a probe molecule, and a Shimadzu FTIR-8101M spectrophotometer. The spectral resolution was 4 cm^{-1}, and 50 scans were coadded. Sample wafers were formed by pressing 20–40 mg of the catalyst at 5 tons/cm^2 and transferred to a quartz sample holder. An inverted T-shaped Pyrex cell containing the sample pellet was used. The two ends of the short arm of the T were fitted with CaF_2 windows. All of the samples were initially outgassed at 723 K for 4 h, and then a background spectrum was recorded after the sample was cooled at room temperature. Data were obtained after admission of pyridine, adsorption at room temperature, and sequential evacuation at 298, 423, 573, and 723 K. Spectra were always recorded at room temperature. Difference spectra were obtained by subtracting the background spectrum recorded previously.

The metal dispersion (D) was determined by chemisorption of hydrogen. Volumetric adsorption experiments were performed at 298 K in a conventional vacuum unit. Catalysts were reduced in H_2 at 673 K for 2 h and then outgassed 2 h at 673 K before gas chemisorption experiments. Hydrogen uptake was determined using the double-isotherm method. After cooling to room temperature, a first isotherm (primary isotherm) was drawn for measuring the total H_2 uptake. Then, and after 1 h of evacuation at room temperature, a second isotherm (secondary isotherm) was performed to determine the amount of weakly adsorbed H_2. The amount of irreversibly held H_2, $(HC)_i$, was calculated as the difference between total and weakly adsorbed H_2. The pressure range of isotherms was 0–6.6 kPa. A stoichiometric atomic ratio of $(HC)_i/M_s = 1$, where M_s implies a metal atom on surface, were used to calculate the metal dispersion.

The crystalline structures of the samples were determined by X-ray diffraction (XRD) using a Shimadzu XD-D1 diffractometer and Ni-filtered Cu$K\alpha$ radiation. BET surface areas (S_g) were measured by N_2 physisorption at its boiling point in a Quantochrome Corporation NOVA-1000 sorptometer. Elemental compositions were measured by atomic absorption spectroscopy (AAS) using a Perkin–Elmer 3110 spectrophotometer.

2.3. Catalytic testing

The liquid-phase hydrogenation of citral (Aldrich, 98%, isomer mixture of 42% *cis* and 58% *trans*) was studied in a Parr 4843 reactor at 343 and 393 K, using isopropanol or toluene (Cicarelli, p.a.) as solvent. The autoclave was loaded with 150 ml of solvent, 10 ml of citral, and 0.2–1 g of catalyst. Before catalytic testing, samples (except Cu/SiO_2) were activated ex situ in pure hydrogen (30 ml/min) for 1 h at 673 K and loaded immediately to the reactor under inert atmosphere. Reduction of Cu/SiO_2 was carried out in pure hydrogen at 523 K to avoid the sintering of Cu^0 crystallites [33]. The reaction system was heated to the reaction temperature at 2 K/min, and the pressure was then rapidly increased to 506.5, 1013, or 2026 kPa with H_2. The liquid-phase conversion of citronellal (Sigma, 95%) was carried out in the same reactor used for citral hydrogenation. The reactor was loaded with 150 ml of toluene, 2 ml of citronellal, and 0.200 g of catalyst previously treated in air for 2 h at 573 K. The reaction was performed at 343 K and 506.5 kPa of nitrogen. Product concentrations were followed during the reaction by ex situ gas chromatography using a Agilent 6850 GC chromatograph equipped with a flame ionization detector, a temperature programmer, and a 30-m Innowax (Agilent) column coupled with a 30-m Supelco α-DEX capillary column. The product analysis was performed using n-dodecane as an external standard. Samples from the reaction system were obtained using a loop under pressure, to avoid flushing. Data were collected every 15–30 min for about 500 min. Conversion of citral (X_{cit}, mol of citral reacted/mol of citral fed) was calculated as $X_{cit} = (C^0_{cit} - C_{cit})/C^0_{cit}$, where C^0_{cit} is the initial concentration of citral and C_{cit} is the concentration of citral at reaction time t. Selectivities (S_j, mol of product j/mol of citral reacted) were calculated as $S_j(\%) = C_j \times 100/\sum C_j$, where C_j is the concentration of product j. Product yields (η_j, mol of product j/mol of citral fed) were calculated as $\eta_j = S_j X_{cit}$.

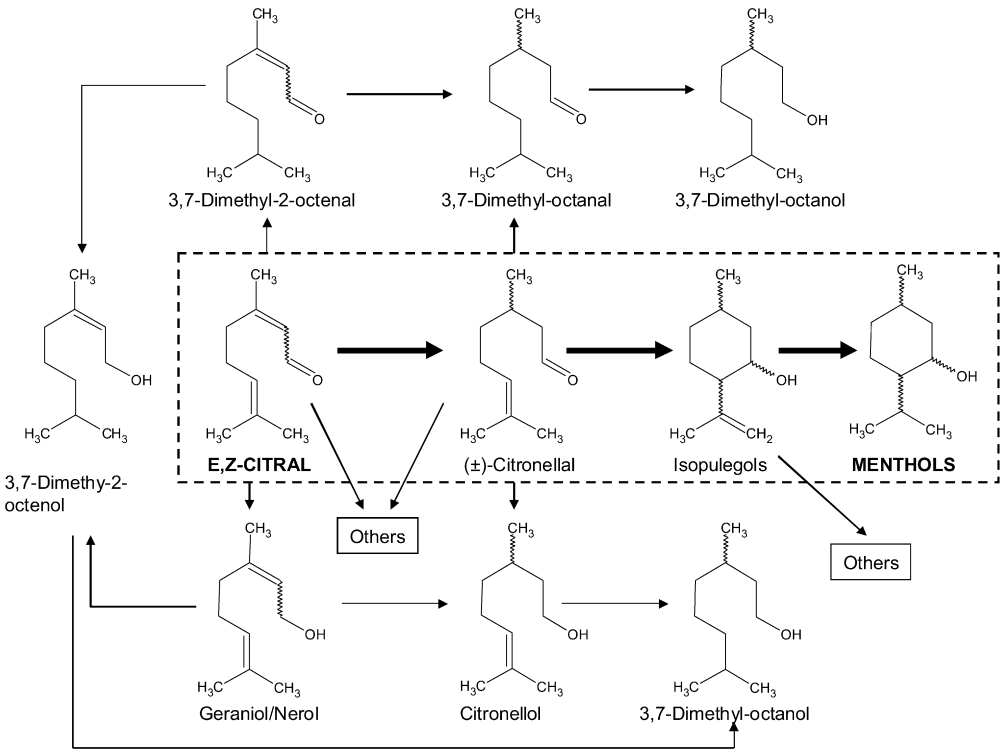

Fig. 1. Reaction network for the synthesis of menthols from citral.

3. Results and discussion

3.1. Reaction network

The one-step synthesis of menthols from citral involves three consecutive steps (Fig. 1): (i) hydrogenation of citral to citronellal; (ii) isomerization/cyclization of citronellal to isopulegol; and (iii) hydrogenation of isopulegol to menthols. Successful selective transformation of citral to menthols requires the development of catalytic materials with the ability to not only promote the coupled hydrogenation/isomerization reactions leading to menthols from citral but also to minimize the parallel reactions leading to undesirable byproducts. For example, hydrogenation of the C=O group or the isolated C=C bond of citral molecule that yield geraniol/nerol and 3,7-dimethyl-2-octenal (3,7-DMEL), respectively, should be avoided to selectively form citronellal from citral. Similarly, the selective production of isopulegol via citronellal cyclization requires prevention of parallel hydrogenation of citronellal to citronellol or to 3,7-dimethyl-octanal (3,7-DMAL). Moreover, citral, citronellal, and isopulegol may form secondary products (identified as "Others" in Fig. 1) via decarbonylation, etherification, and cracking reactions, which will also affect the synthesis of menthols in high yields.

To develop bifunctional metal/acid catalysts that are active and selective for menthol synthesis, we initially studied here the individual steps involved in the reaction pathway leading to menthols from citral in Fig. 1. Specifically, we investigated the hydrogenation of citral to citronellal on several silica-supported metals and the isomerization of citronellal to isopulegols on different solid acids.

3.2. Citral hydrogenation

The hydrogenation of citral to citronellal was investigated on silica-supported metals containing about 12% of a nonnoble metal (Ni, Co, or Cu) or between 0.3 and 1.0% of a noble metal (Pd, Pt, or Ir). The metal loadings and the physical properties of these catalysts, together with the results of catalyst characterization by different techniques, are given in Table 1. The BET surface area of the silica support (230 m^2/g) did not change significantly after the metal impregnation and the consecutive oxidation/reduction steps used for obtaining metal/SiO_2 catalysts. After calcination in air at 673 K for decomposing metal nitrate precursors, samples were characterized by XRD. NiO (ASTM 4-835), CuO (ASTM 5-0661), and Co_3O_4 (ASTM 9-418) were identified on Ni/SiO_2, Cu/SiO_2, and Co/SiO_2 catalysts, respectively (Table 1). In contrast, the XRD diffractograms of noble metal/SiO_2 catalysts did not show the presence of crystalline metal oxides, probably because of the low metal content. Sample characterization by TPR (Table 1) showed that reduction of NiO and CuO on silica gives rise to single TPR peaks centered at 663 and 523 K, respectively, corresponding to the direct reduction of Ni^{2+} and Cu^{2+} ions to Ni^0 and Cu^0. On Ni/SiO_2, we found no reduction peak at higher temperatures that would reveal the presence of less-reducible surface Ni silicates. The TPR profile of Co_3O_4 on silica exhibited two reduction peaks at 577 and 653 K, which reflect the consecutive reduction $Co^{3+} \rightarrow Co^{2+} \rightarrow Co^0$ [34,35]. Palladium and iridium oxides on silica were reduced at about 400 K, whereas no reduction peak was observed for the Pt/SiO_2 sample. This last result strongly suggests that decomposition of $Pt(NH_3)_4(OH)_2$ precursor in nitrogen caused the reduction

Table 1
Characterization of silica-supported catalysts used for citral hydrogenation reaction

Catalyst	Metal loading (%)	S_g (m^2/g)	Oxide particle size[a] (nm)	TPR T_{max} (K)	H_2 chemisorption $(HC)_i$ (l STP/mol metal)	Metal dispersion (%)
Ni/SiO_2	11.8	250	32 (NiO)	663	0.53	5
Cu/SiO_2	12.5	220	20 (CuO)	523	0.08	–
Co/SiO_2	12.3	240	21 (Co_3O_4)	577, 653	0.16	–
Pt/SiO_2	0.3	260	–	n.d.[b]	1.49	27
Pd/SiO_2	0.7	250	–	393	1.98	17
Ir/SiO_2	1.0	230	–	403	1.81	16

[a] Determined by XRD.
[b] n.d: not detected.

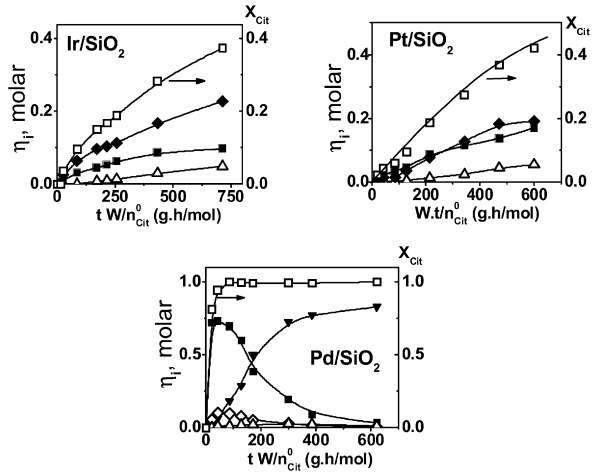

Fig. 2. Citral hydrogenation. Product yields and citral conversion as a function of parameter tW/n^0_{cit} for Pt/SiO_2, Ir/SiO_2, and Pd/SiO_2 catalysts. (■) Citronellal, (◆) geraniol/nerol, (△) Citronellol, (▼) 3,7-DMAL, (◇) 3,7-DMEL [393 K, 1013 kPa hydrogen, $W = 1$ g, citral/isopropanol = 2:150 (ml).]

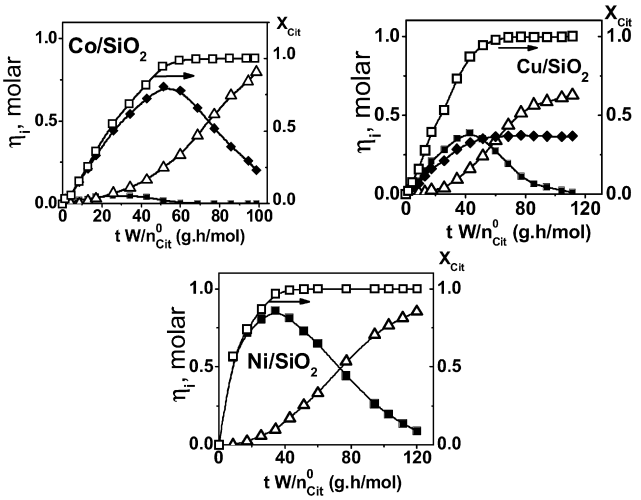

Fig. 3. Citral hydrogenation. Product yields and citral conversion as a function of parameter tW/n^0_{cit} for Co/SiO_2, Cu/SiO_2, and Ni/SiO_2 catalysts. (■) Citronellal, (◆) geraniol/nerol, (△) citronellol. Reactions conditions as in Fig. 2.

of platinum to Pt^0, which is in agreement with previous work reporting that NH_3 is released during $Pt(NH_3)_4(OH)_2$ decomposition under inert atmospheres and reduces PtO to metallic Pt [36,37]. Taking into account the above TPR results, it is inferred that on all of the silica-supported catalysts used in this work, the metal fraction is totally in the metallic state after the standard reduction step used in the catalyst preparation procedure (reduction in pure H_2 at 523 K for Cu/SiO_2 and at 673 K for the rest of metal/SiO_2 samples). The metallic fraction of reduced catalysts was characterized by hydrogen chemisorption (Table 1). The adsorbed amount of irreversible H_2 was used to calculate the metal dispersion of Pt/SiO_2, Pd/SiO_2, Ir/SiO_2, and Ni/SiO_2 samples, using a H:metal = 1 adsorption stoichiometry. It is known that the H_2 chemisorption is not suitable for determining the metal dispersion of Cu(Co)-based catalysts.

Samples were tested for citral conversion reactions at 393 K using as solvent isopropanol, a polar compound. Only products formed via citral hydrogenation reactions were observed. The main reaction products were citronellal, geraniol/nerol, citronellol, and 3,7-DMAL; minor amounts of 3,7-DMEL were also detected. Fig. 2 shows the product yields (η_i) for noble metal/SiO_2 catalysts as a function of tW/n^0_{cit}, where t is the reaction time, W is the catalyst weight, and n^0_{cit} is the initial moles of citral. Similar plots for silica-supported nonnoble metal catalysts are presented in Fig. 3. The local slopes of the curves in Figs. 2 and 3 give the rate of formation of each product at a specific value of citral conversion and reaction time. In all cases, citronellal, geraniol/nerol, and 3,7-DMEL presented nonzero initial slopes, indicating that they are primary products. In contrast, the zero initial slopes observed for the other detected products (citronellol, 3,7-DMAL) suggest that these compounds are secondary products. These results are consistent with the reaction network proposed in Fig. 1 for citral conversion reactions.

Fig. 2 shows that the initial conversion rate of citral was clearly higher on Pd/SiO_2 than on Ir/SiO_2 or Pt/SiO_2. The Ir/SiO_2 catalyst formed mainly geraniol/nerol, indicating that iridium catalyzes preferentially the C=O bond of citral and thus is not selective for producing citronellal. On Pt/SiO_2, the initial formation rates of citronellal and geraniol/nerol were similar, and both products were then hydrogenated to citronellol. Formation of small amounts of 3,7-DMAL were also detected on Pt/SiO_2 for citral conversions >30%. In contrast, Pd/SiO_2 essentially hydrogenated the conjugated C=C bond of citral, producing initially citronellal with >95% selectivity. This catalyst was also active for hydrogenating the nonconjugated C=C bond and initially formed minor amounts of 3,7-DMEL from citral, but then transformed almost completely citronellal to 3,7-DMAL.

Overall, our results are consistent with previous works on citral hydrogenation over noble metals. For example, Singh and Vannice [20] found that under the initial conditions, both the citral hydrogenation turnover rate and selectivity to citronellal were clearly higher on Pd/SiO_2 than on Ir/SiO_2 or Pt/SiO_2, whereas Aramendía et al. [19] reported that Pd is active for hydrogenating citronellal to 3,7-DMAL. Reyes et al. [13] studied the liquid-phase citral hydrogenation on Ir supported on SiO_2 and TiO_2 modified by the presence of Fe and Ge additives. In agreement with our results of Fig. 2, they reported that at 10% citral conversion, all of the Ir-based catalysts formed predominantly geraniol/nerol. On the other hand, Vilella et al. [38] observed that the selectivities to citronellal and to unsaturated alcohols (nerol and geraniol) were similar when compared at low citral conversions on Pt/carbon catalysts, which is consistent with our results shown for Pt/SiO_2 in Fig. 2.

Regarding nonnoble metal catalysts, Fig. 3 shows that Co/SiO_2 selectively promoted the initial hydrogenation of citral to nerol/geraniol isomers, which were then transformed to citronellol. Citronellal was formed in minor amounts on Co/SiO_2, reaching a maximum selectivity of about 15%. The initial formation rates of citronellal and geraniol/nerol were similar on Cu/SiO_2, but whereas the geraniol/nerol yield remained constant after total conversion of citral, citronellal was consecutively hydrogenated to citronellol. Finally, on Ni/SiO_2, citral was initially transformed almost exclusively to citronellal, giving an initial citral selectivity close to 100%. The selectivity to citronellal then decreased with reaction time, because citronellal was in turn hydrogenated to citronellol. The high selectivity observed here on Ni/SiO_2 for hydrogenating the conjugated C=C bond of citral molecule is in agreement with previous results reported on Ni Raney [39] and Ni/Al_2O_3 [40]. It must be noted that nonnoble metals were not active for hydrogenating the isolated C=C bond of citral, in contrast with the significant formation of 3,7-DMEL and 3,7-DMAL observed on Pd and to a lesser extent on Pt.

The differences in the relative hydrogenation rates of the C=O and C=C bonds of citral on silica-supported metal catalysts may be interpreted by taking into account the attractive and repulsive forces existing between the emergent d-orbitals of the metal and the C=C and the C=O groups of the adsorbate. In fact, the factors governing intrinsic metal selectivities have been qualitatively related to the d-band width using extended Hückel calculations [41,42]. The adsorbate adsorption strength would be determined by the balance between attractive two-electron interactions and repulsive four-electron interactions. The wider the metal d-band, the stronger the repulsive four-electron interactions and the lower the interaction between the C=C conjugated bond and the metal surface. In the case of our nonnoble metal catalysts, for example, the significant extent of Co d-orbitals in Co/SiO_2 would increase the electrostatic repulsion between the metal surface and the conjugated C=C bond of citral, thereby favoring citral adsorption via its carbonyl group and the formation of the unsaturated alcohol. In contrast, Ni has a narrower d-band width compared with Co and does not hydrogenate the C=O bond of citral forming essentially citronellal. A similar explanation may account for the higher initial citronellal selectivity observed on Pd compared with Ir or Pt, because Pd has the narrowest d-band width.

In summary, our results in Figs. 2 and 3 show that only Pd and Ni preferentially hydrogenate the C=C bond of citral and exhibit initial selectivities to citronellal of about 100%. Taking into account that the rapid and selective transformation of citral to citronellal is the first requisite to fulfill for the reaction pathway leading from citral to menthols (Fig. 1), we preliminary selected these two metals for the bifunctional catalyst formulations.

3.3. Citronellal isomerization

The citronellal isomerization to isopulegols was studied on ZnO/SiO_2, SiO_2–Al_2O_3, Al-MCM-41, CsHPA, and zeolites HBEA and HZSM5. The chemical composition and physical properties of these samples are given in Table 2. The XRD pattern of Al-MCM-41 shows a sharp diffraction peak at 2.14 degrees and two smaller peaks at 3.7 and 4.3 degrees, corresponding to 100, 110, and 200 reflections, respectively, confirming the hexagonal structure of this mesoporous material.

Sample acid properties were probed by TPD of NH_3 preadsorbed at 373 K and by infrared spectroscopy using pyridine as the probe molecule. The obtained TPD profiles of NH_3 are shown in Fig. 4. The NH_3 evolved from HZSM5 gives rise to a peak at about 531 K and a broad band at higher temperatures. HBEA and SiO_2–Al_2O_3 do not exhibit the high-temperature NH_3 band, but do show a single asymmetric broad band with a maximum at around 613 K. Similarly, the TPD profiles of ZnO/SiO_2 and Al-MCM-41 consist of an asymmetric broad band with a maximum at lower temperatures (ca. 550 K). The TPD curve of CsHPA presents a high-temperature peak at about 883 K that accounts for the strong Brönsted acid sites present on this material. Acid site densities (μmol/g or

Table 2
Chemical composition and physical properties of the samples used for citronellal isomerization

Catalyst	Si/Al	Zn (%)	Cs (%)	Surface area S_g (m^2/g)	Pore diameter $\bar{d}_p$ (Å)
HZSM5	20.0	–		350	5.5
HBEA	25.0	–		608	6.7
SiO_2–Al_2O_3	16.0	–		540	51
Al-MCM-41	10.0	–		780	30
ZnO/SiO_2	–	20		125	120
CsHPA	–		10	140	–

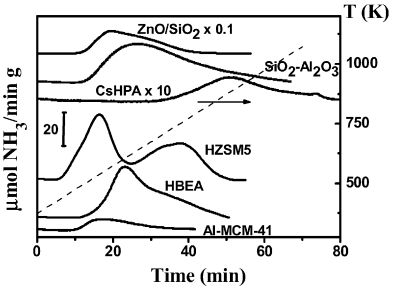

Fig. 4. TPD profiles of NH_3—heating rate: 10 K/min.

Table 3
Acidity characterization of the samples used for citronellal isomerization

Catalyst	TPD of NH_3		IR of pyridine		
	(μmol/g)	(μmol/m^2)	Brönsted sites (B)[a] (area/g)	Lewis sites (L)[a] (area/g)	$L/(L+B)$
HZSM5	770	2.2	337	341	0.50
HBEA	500	0.8	150	151	0.50
SiO_2–Al_2O_3	1030	1.8	68	204	0.75
Al-MCM-41	110	0.2	20	36	0.64
ZnO/SiO_2	2240	18	0	51	1
CsHPA	37	0.3	–	–	–

[a] Determined from IR spectra after sample evacuation at 423 K.

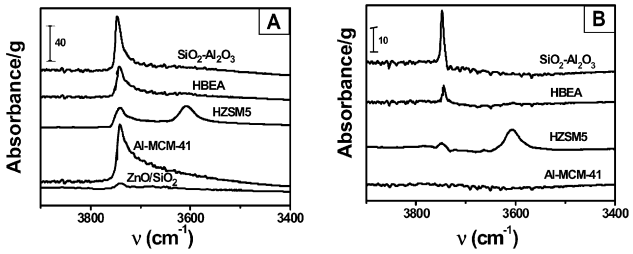

Fig. 5. IR spectra in the hydroxyls stretching region: (A) samples degassed at 723 K for 4 h, (B) difference spectra between the matrix spectra in (A) and the spectra obtained after pyridine adsorption at room temperature and desorption at 423 K.

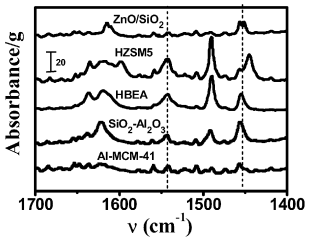

Fig. 6. IR spectra of pyridine adsorbed at 298 K and evacuated at 423 K for 0.5 h. Dotted lines indicate the presence of Lewis (1450 cm^{-1}) and Brönsted (1540 cm^{-1}) sites.

μmol/m^2 of evolved NH_3) were calculated by deconvolution and integration of TPD traces and are presented in Table 3. On an areal basis, ZnO/SiO_2 exhibits the highest surface acid density (about 18 μmol/m^2), followed by HZSM5 (2.2 μmol/m^2), SiO_2–Al_2O_3 (1.8 μmol/m^2), HBEA (0.8 μmol/m^2), CsHPA (0.3 μmol/m^2), and Al-MCM-41 (0.2 μmol/m^2).

Fig. 5A shows the FTIR spectra of the samples in the hydroxyl-stretching region obtained after evacuation at 723 K for 4 h. The positions of the IR band for the O–H stretching modes (ν_{OH}) over degassed Al-MCM-41 and SiO_2–Al_2O_3 are almost the same, at about 3745 cm^{-1}. No absorption bands are seen in hydroxyl stretching on ZnO/SiO_2, indicating that the hydroxyl group concentration is negligible on this sample. The spectrum of degassed zeolite HZSM5 shows two absorption bands at 3610 and 3745 cm^{-1}. The band at 3610 cm^{-1} corresponds to Si–OH–Al bridging hydroxyl groups [43], whereas the asymmetric band at 3745 cm^{-1} is attributed to the stretching vibration of terminal SiOH groups located either at the boundaries of the zeolite crystal or at the surface of noncrystalline material [44]. Zeolite HBEA presents the band for silanol groups at about 3745 cm^{-1} [45,46]. A weak, wide band at 3605–3610 cm^{-1} indicates the presence of bridged OH groups [46,47].

The ν_{OH} wavenumber of the samples in Fig. 5A is not straightforwardly related to the acid strength of the hydroxyl group [48]. More useful information on Brönsted acid site strength is obtained by analyzing the difference spectra between the matrix spectra of Fig. 5A and those obtained after pyridine adsorption at room temperature and desorption at 423 K (Fig. 5B). In fact, it is observed that after desorption at 423 K of the pyridine adsorbed at room temperature, the base is almost completely eliminated on Al-MCM-41 but remains significantly adsorbed on SiO_2–Al_2O_3. This finding reflects the stronger acidity of surface OH groups on SiO_2–Al_2O_3 compared with Al-MCM-41. On the other hand, Fig. 5B shows that evacuation of HZSM5 at 423 K does not significantly remove the pyridine adsorbed at room temperature on bridging OH at 3610 cm^{-1}, reflecting the strong adsorption of pyridine on Si–OH–Al groups of zeolite HZSM5. In contrast, the interaction of pyridine with terminal silanol OH groups at 3745 cm^{-1} is very weak. Finally, weakly acidic SiOH groups of zeolite HBEA at 3743 cm^{-1} are affected by pyridine adsorption, probably because of a perturbation of these groups by the pyridine molecules adsorbed on neighboring Lewis sites [49].

The nature and density of surface acid sites were determined from the IR spectra obtained after admission of pyridine at room temperature and sequential evacuation at 298, 423, 573, and 723 K. The pyridine absorption bands at around 1540 cm^{-1} and between 1440 and 1460 cm^{-1} arise from pyridine adsorbed on Brönsted and Lewis acid sites, respectively, on zeolites [50–53], Al-MCM-41 [53,54], and SiO_2–Al_2O_3 [55]. Fig. 6 shows the IR spectra obtained on HBEA, HZSM5, Al-MCM-41, ZnO/SiO_2, and SiO_2–Al_2O_3 after pyridine evacuation at 423 K. We decided to compare the sample IR spectra at 423 K because those collected after evacuation at 298 K contained broad absorption bands characteristic of the presence of physisorbed pyridine. The relative contributions of Lewis and Brönsted acid sites were obtained by deconvolution and integration of pyridine absorption bands appearing in Fig. 6 at around 1450 and 1540 cm^{-1}, respectively. Results are given in Table 3. On zeolite HZSM5, the band of adsorbed pyridine on Lewis acid sites is split into two overlapping peaks at 1445 and 1455 cm^{-1}, respectively. A similar two peak band for the pyridine adsorption on Lewis acid sites on HZSM5 has been reported by others [56], who suggested that the Lewis acidity on

HZSM5 is due to Al located in the zeolite framework, probably generated during calcination, resulting in partial hydrolysis of Al–O bonds. The amounts of pyridine adsorbed on Brönsted and Lewis sites of zeolite HZSM5 were similar ($L/B \cong 1$) after evacuation at 423 K (about 340 area/g) and 723 K (150–160 area/g). The significant amounts of pyridine present on HZSM5 after evacuation at high temperatures indicated that it contains strong Lewis and Brönsted acid sites. On HBEA, the pyridine adsorbed on Brönsted and Lewis acid sites appear at 1542 and 1455 cm^{-1}, respectively. The amounts of pyridine adsorbed on both Lewis and Brönsted sites of HBEA are significantly lower than those adsorbed on HZSM5, confirming that zeolite HBEA is less acidic than HZSM5, as suggested by the TPD profiles of NH_3 in Fig. 4. The L/B ratio determined on HBEA at 423 K was close to 1. On the other hand, the IR spectra of Fig. 6 show that on Al-MCM-41 and SiO_2–Al_2O_3, the coordinately bound pyridine band appears at 1455 cm^{-1}, reflecting the adsorption of pyridine on Lewis acid sites associated with tricoordinate Al atoms. In agreement with the results obtained by TPD of NH_3, the amount of pyridine adsorbed on Al-MCM-41 after evacuation at 423 K is clearly lower compared with that on zeolites or SiO_2–Al_2O_3, reflecting the moderate acidic character of the mesoporous Al-MCM-41 sample. Pyridine is almost completely eliminated on Al-MCM-41 after evacuation at 723 K. The $L/(L + B)$ ratio is higher on SiO_2–Al_2O_3 than on Al-MCM-41 (Table 3). Finally, the pyridine absorption spectrum on sample ZnO/SiO_2 does not show the presence of surface Brönsted sites, consistent with the IR characterization of hydroxyl groups in Fig. 5A. Moreover, the amount of pyridine remaining on ZnO/SiO_2 after evacuation at 423 K is clearly lower compared with zeolites or SiO_2–Al_2O_3 (Table 3), despite the fact that ZnO/SiO_2 exhibits the highest surface acid density on TPD of NH_3 (Table 3). This result demonstrates that ZnO/SiO_2 contains mainly weak Lewis acid sites.

The liquid-phase citronellal cyclization to isopulegols was studied on the samples listed in Table 2 using toluene as a solvent because preliminary catalytic tests on ZnO/SiO_2 showed that the reaction is almost completely inhibited when isopropanol is the solvent. The citronellal conversion and isopulegol yield as a function of parameter tW/n^0_{clal} are represented in Figs. 7A and 7B, respectively. Fig. 7A shows that the citronellal cyclization rate is clearly lower on ZnO/SiO_2 and CsHPA samples compared with Al-MCM-41, SiO_2–Al_2O_3, or zeolite HBEA. On the other hand, citronellal conversion is very low on zeolite HZSM5, in line with previous results reported by Mäki-Arvela et al. [57]. These authors considered that the poor activity of zeolite HZSM5 for this reaction is essentially due to diffusional limitations of the product in the narrow pore structure. Cyclization of citronellal has been investigated on different solid acids, including zeolites [24], SiO_2–Al_2O_3 and SiO_2–TiO_2 mixed oxides [58], hydrous and sulfated zirconia [25], and $ZnBr_2/SiO_2$ [59]. The exact nature of the surface active sites required to efficiently catalyze the cyclization of citronellal to isopulegols remains under debate. Although several authors [58,59] have reported that the reaction is readily catalyzed on Lewis acids, others [24] have correlated the cyclization activity on acid zeolites with accessible Brönsted acid sites. Chuah et al. [25] found that catalytic materials containing strong Lewis and weak Brönsted acidity show good activity and selectivity for cyclization of citronellal to isopulegol. They consequently proposed a cyclization mechanism based on the coordination of the citronellal to a strong Lewis site, followed by protonation from a Brönsted acid site. Our results in Fig. 7 show that the samples containing exclusively Lewis (ZnO/SiO_2) or strong Brönsted acid sites (CsHPA) are less active for citronellal isomerization than those samples exhibiting dual Lewis/Brönsted acidity, such as SiO_2–Al_2O_3, Al-MCM-41, and zeolite HBEA. Moreover, whereas on SiO_2–Al_2O_3, Al-MCM-41, and HBEA the yields of isopulegols at the end of the runs are >90%, ZnO/SiO_2 and CsHPA form significant amount of byproducts, giving isopulegol yields of around 72% (Fig. 7B).

In brief, taking into account that SiO_2–Al_2O_3, Al-MCM-41, and zeolite HBEA showed the highest initial formation rate of isopulegols, we preliminary selected them as the acidic components of our bifunctional catalyst formulations.

3.4. One-step synthesis of menthols from citral

Based on the results of Figs. 2, 3, and 7, we studied the conversion of citral to menthols on bifunctional catalysts containing one of the metals most selective for hydrogenating citral to citronellal (Pd or Ni) and one of the solid acids more active for converting citronellal to isopulegols (zeolite HBEA, SiO_2–Al_2O_3, or Al-MCM-41). Initially, we prepared Pd (1%) supported on zeolite HBEA (Pd/HBEA) and Ni (3%) supported on zeolite HBEA (Ni/HBEA), SiO_2–Al_2O_3 (Ni/SiO_2–Al_2O_3), and Al-MCM-41 (Ni/Al-MCM-41). The physical properties (surface area, metal dispersion) as well as the surface acidity of these catalysts are given in Table 4. Comparing results given in Tables 2, 3, and 4, we can infer that the addition of metal slightly diminished the surface area of the supports but did not change their ammonia adsorption capacity. The catalysts listed

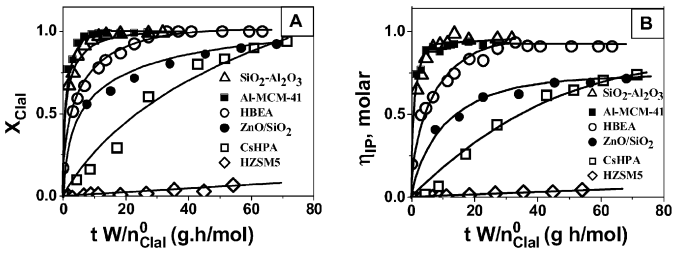

Fig. 7. Citronellal isomerization. Citronellal conversion (A) and isopulegols yield (B) and as a function of parameter tW/n^0_{clal}. [343 K, $W = 0.2$ g, citronellal/toluene = 2:150 (ml).]

Table 4
Citral to menthols: Physical and acid properties of the samples

Catalyst	Surface area S_g (m^2/g)	Metal (wt%)	Metal dispersion (%)	TPD NH_3 (μmol/m^2)
Pd/HBEA	560	1	57.0	0.8
Ni/HBEA	550	3	4.6	0.8
Ni/SiO_2–Al_2O_3	540	3	12.0	1.7
Ni/Al-MCM-41	740	3	6.0	0.2
Ni(8%)Al-MCM-41	720	8	3.8	0.2

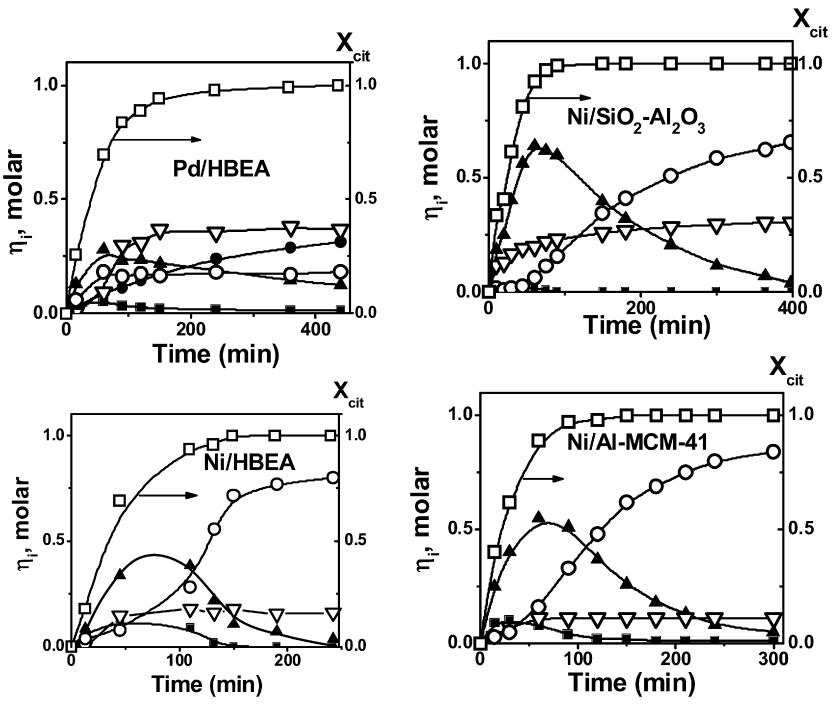

Fig. 8. Citral to menthols. Product yields and citral conversion as a function of time for Pt/HBEA, Ni/HBEA, Ni/SiO_2–Al_2O_3 and Ni/Al-MCM-41 catalysts. (○) Menthols, (▲) isopulegols, (■) citronellal, (▽) others, (●) 3,7-DMAL. [343 K, 506.5 kPa, $W = 1$ g, citral/toluene = 2:150 (ml).]

in Table 4 were tested for the conversion of citral to menthols at 343 K and $P_{H_2} = 506.5$ kPa, using 1 g of sample and toluene as a solvent. Catalytic results are given in Fig. 8. In all the cases, citral and citronellal were totally converted after about 3 h of reaction.

Pd/HBEA produced significant amounts of undesirable 3,7-dimethyl-octanal, demonstrating that the hydrogenation rate of the C=C bond of citronellal on Pd is comparable to the citronellal isomerization rate on surface acid sites. Formation of "others" (see the reaction network in Fig. 1), probably arising from citral and citronellal secondary reactions, was also important on Pd/BEA. Moreover, isopulegols were not totally converted to menthols after 7 h of reaction, reflecting the poor activity of Pd for hydrogenating the C=O bond, as can be inferred from the results obtained on monofunctional Pd/SiO_2 in Fig. 2. Thus, the menthol yield at the end of the run was only about 20%, showing that bifunctional Pd/HBEA cannot selectively convert citral to menthols in a one-step process.

Ni/HBEA was clearly more selective to menthols than Pd/HBEA, essentially because the formation of 3,7-dimethyl-octanal from citronellal was negligible on Ni/HBEA. This is consistent with results in Fig. 3 showing that Ni may selectively hydrogenate the conjugated C=C bond of citral but is practically inactive to hydrogenate the isolated C=C group. Actually, none of the byproducts formed from hydrogenation of citral or citronellal (Fig. 1) was detected using Ni/HBEA, suggesting that this bifunctional catalyst satisfactorily combines the hydrogenation and isomerization functions needed to selectively promote the reaction pathway leading from citral to menthols. However, the yield to menthols at the end of the catalytic run was only about 81%, because Ni/HBEA formed significant amounts of secondary compounds, probably via decarbonylation and cracking of citral and citronellal on the strong acid sites of zeolite HBEA. The menthol isomer distribution on Ni/HBEA was 72.0% (±)-menthols, 21.3% (±)-neomenthol, and 6.7% (±)-isomenthols. Catalyst Ni/SiO_2–Al_2O_3 was more acid than Ni/HBEA and formed about 31% of "others" at the end of the catalytic run, thereby causing the menthol yield to reach only 66%.

The best catalyst was Ni/Al-MCM-41, which yielded about 89% of menthols after the 300-min run. As shown in Fig. 8, citral was totally converted to citronellal on Ni/Al-MCM-41 in about 80 min, but the concentration of citronellal always remained very low, because it was readily converted to isopulegols on acid sites of mesoporous Al-MCM-41 support. Isopulegols were then totally hydrogenated to menthols on metal Ni surface sites. The observed menthol yield improvement on Ni/Al-MCM-41 compared with Ni/HBEA or Ni/SiO_2–Al_2O_3 can be explained by considering that the moderate acidity of Al-MCM-41 does not promote the formation of byproducts via side-cracking reactions. Regarding the distribution of menthol isomers, on Ni/Al-MCM-41 the menthol mixture was composed of 72.3% of (±)-menthols, 20.2% of (±)-neomenthols, and 7.5% of (±)-isomenthol.

To further improve the production of menthols observed in Fig. 8 on Ni/Al-MCM-41, we explored the effect of increasing both the amount of Ni on the catalyst and the hydrogen pressure on menthol yield. Results obtained at 2026.0 kPa on the standard Ni/Al-MCM-41 containing 3% Ni and on a Ni(8%)/Al-MCM-41 are given in Table 5 and compared with those extracted from Fig. 8 for Ni/Al-MCM-41 at 506.5 kPa. It is observed that the initial citral conversion rate (r^0_{cit}, mol/h g_{cat}) on Ni/Al-MCM-41 sample increased from 0.0176 to 0.0370 mol/h g_{cat} when the H_2 pressure was increased from

Table 5
Citral to menthols: Initial reaction rates, product yields, and menthol isomers on Ni/Al-MCM-41 catalysts

Catalyst	Pressure (kPa)	r^0_{cit} [a] (mol/h g_{cat})	Yield (%)[b]			Menthol isomer distribution (%)[b]		
			Menthols	Isopulegols	Others	(±)-menthols	(±)-neomenthols	(±)-isomenthols
Ni/Al-MCM-41	506.5	0.0176	89.2	0	10.8	72.3	20.2	7.5
Ni/Al-MCM-41	2026.0	0.0370	93.0	0	7.0	70.1	20.0	8.9
Ni(8%)/Al-MCM-41	2026.0	0.0600	94.0	0	6.0	71.0	20.0	8.0

Note. $T = 343$ K, $W = 1$ g, citral:toluene = 2:150 (ml).
[a] Initial citral conversion rate.
[b] Values determined at 300 min reaction; $X_{cit} = 100\%$ on all catalysts.

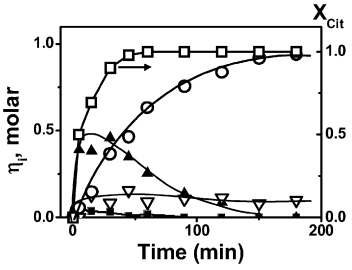

Fig. 9. Citral to menthols. Product yields and citral conversion as a function of time for Ni(8%)/Al-MCM-41 catalyst. (○) Menthols, (▲) isopulegols, (■) citronellal, (▽) others. [343 K, 2026.0 kPa, $W = 1$ g, citral/toluene = 2:150 (ml).]

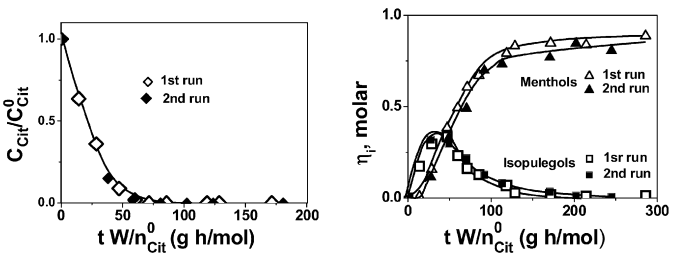

Fig. 10. Citral to menthols. Consecutive in situ catalytic runs to evaluate catalyst deactivation. Sample: Ni(8%)/Al-MCM-41. Reactions conditions as in Fig. 9.

506.5 to 2026.0 kPa. Moreover, the H_2 pressure increase diminished the formation of "others" on Ni/Al-MCM-41 and augmented the menthol yield from 89.2 to 93.0% without significantly changing the menthol isomer distribution. Table 5 also shows that r^0_{cit} increased significantly when the amount of Ni on Al-MCM-41 was increased from 3 to 8%. In this regard, Fig. 9 shows the evolution of product yields and citral conversion as a function of time obtained on the Ni(8%)/Al-MCM-41 sample. Although from Table 5 it can be inferred that the menthol yields obtained on Ni/Al-MCM-41 and Ni(8%)/Al-MCM-41 samples at 2026.0 kPa are practically the same, Fig. 9 shows that Ni(8%)/Al-MCM-41 completely transformed isopulegols to menthols in about 150 min, whereas Ni/Al-MCM-41 required 300 min. In other words, menthol productivity (expressed as mol menthol/g h) was two times higher on Ni(8%)/Al-MCM-41 than on Ni/Al-MCM-41. The observed increase in menthol productivity with Ni loading seems to essentially reflect the increase in the isopulegol hydrogenation rate to menthols.

Finally, we studied the deactivation of Ni(8%)/Al-MCM-41 by performing two consecutive catalytic tests without stopping the run. The procedure was as follows: Immediately after isopulegols were completely transformed to menthols in a standard run at 2026.0 kPa, we introduced to the reactor (without opening it) the same amount of initial moles of citral, n^0_{cit}, and performed a second consecutive run. The results, shown in Fig. 10, indicate that the citral concentration decay rate and the evolution of menthol yield with time were practically the same for both consecutive catalytic tests. Thus, the results of Fig. 10 demonstrate that the in situ deactivation of Ni(8%)/Al-MCM-41 during the total conversion of citral to menthols at 2026.0 kPa was very low.

In summary, Ni supported on Al-MCM-41 is a stable, highly selective catalyst for the one-pot transformation of citral to menthols that yields >90% of menthols and produces about 72% of racemic (±)-menthol in the menthol mixture.

4. Conclusions

The one-pot synthesis of menthols from citral may be successfully achieved using bifunctional metal/acid catalysts with the ability to selectively promote the required reaction pathway: (i) hydrogenation of citral to citronellal; (ii) cyclization of citronellal to isopulegols; and (iii) hydrogenation of isopulegols to menthols. The initial citronellal formation rate from citral is clearly higher on Pd and Ni compared with other noble (Pt, Ir) or nonnoble (Cu, Co) metals. The narrower *d*-band width of Ni and Pd compared with the other metals decreases the electrostatic repulsion between the metal surface and the conjugated C=C bond of citral, thereby favoring citral adsorption via its C=C bond and citronellal formation.

Citronellal may be converted to isopulegols on catalysts containing only Lewis (ZnO/SiO_2) or strong Brönsted (CsHPA) acid sites, but isopulegols are obtained more selectively using solids exhibiting dual Brönsted/Lewis acidity, such as zeolite HBEA, SiO_2–Al_2O_3, or Al-MCM-41. However, isopulegol formation is severely hampered on zeolite HZSM5 because of diffusional constraints.

Palladium supported on acid supports does not selectively form menthols from citral, because palladium hydrogenates the nonconjugated C=C bond of citronellal intermediate at a high rate, producing considerable amounts of undesirable 3,7-dimethyl-octanal. In contrast, bifunctional Ni/solid acid catalysts form essentially menthols from citral and give 70–75% of racemic (±)-menthol in the menthol mixture. Acid supports of moderate acidity, such as Al-MCM-41, lead to higher menthol yields than zeolite HBEA or SiO_2–Al_2O_3, because the presence of strong acid sites promotes the formation of unwanted byproducts. Ni(8%)/Al-MCM-41 at 2026.0 kPa hydro-

gen yields >90% menthols with no significant activity decay after two consecutive catalytic tests.

Acknowledgments

This work was supported by the Universidad Nacional del Litoral (UNL), Consejo Nacional de Investigaciones Científicas y Técnicas (CONICET), and Agencia Nacional de Promoción Científica y Tecnológica (ANPCyT), Argentina.

References

[1] G.S. Clark, Menthol Perfurm. Flavor. 25 (1998) 33.
[2] J. Fleischer, K. Bauer, R. Hopp, DE 2109456, Harrmann & Reimer, 1971.
[3] J.C. Davis, Chem. Eng. 11–12 (1978) 62.
[4] S. Otsuka, K. Tani, T. Yamagata, S. Akutagawa, H. Kumobayashi, M. Yagi, EP 68506, Takasago, 1982.
[5] M. Misono, N. Nojiri, Appl. Catal. 64 (1990) 1.
[6] A. Trasarti, A.J. Marchi, C.R. Apesteguía, J. Catal. 224 (2004) 484.
[7] P.Z. Bedoukian, Perfumery and Flavoring Synthetics, Elsevier, New York, 1967, p. 99.
[8] A. Chauvel, B. Delmon, W.F. Holderich, Appl. Catal. A 115 (1994) 173.
[9] S. Recchia, C. Dossi, N. Poli, A. Fussi, L. Sordelli, R. Psaro, J. Catal. 184 (1999) 1.
[10] L. Sordelli, R. Psaro, G. Vlaic, A. Cepparo, S. Recchia, C. Dossi, A. Fussi, R. Zanoni, J. Catal. 182 (1999) 186.
[11] J.N. Coupé, E. Jordão, M.A. Fraga, M.J. Mendes, Appl. Catal. A Gen. 199 (2000) 45.
[12] C.F. Santori, M.L. Casella, G.J. Siri, H.R. Aduriz, O.A. Ferretti, Appl. Catal. A Gen. 197 (2000) 141.
[13] P. Reyes, H. Rojas, G. Pecchi, J.L.G. Fierro, J. Mol. Catal. A Chem. 179 (2002) 293.
[14] S. Galvagno, C. Milone, A. Donato, G. Neri, R. Pietropaolo, Catal. Lett. 17 (1993) 55.
[15] G. Neri, C. Milone, A. Donato, L. Mercadante, A.M. Visco, J. Chem. Technol. Biotechnol. 60 (1994) 83.
[16] T. Salmi, P. Mäki-Arvela, E. Toukoniitty, A. Kalantar Netestanaki, L.-P. Tiainen, L.-E. Lindfors, R. Sjöholm, E. Laine, Appl. Catal. A Gen. 196 (2000) 93.
[17] G. Lafaye, T. Ekou, C. Micheaud-Especel, C. Montassier, P. Marecot, Appl. Catal. A Gen. 257 (2004) 107.
[18] R. Hubaut, J.P. Bonelle, M. Daage, J. Molec. Catal. 55 (1989) 170.
[19] M.A. Aramendía, V. Borau, C. Jiménez, J.M. Marinas, A. Porras, F.J. Urbano, J. Catal. 172 (1997) 46.
[20] U.K. Singh, M.A. Vannice, J. Catal. 199 (2001) 73.
[21] B.C. Clark Jr., T.S. Chamblee, G.A. Iacobucci, J. Org. Chem. 49 (1984) 4557.
[22] V.K. Aggarwal, G.P. Vennall, P.N. Davey, C. Newman, Tetrahedron Lett. 39 (1998) 1997.
[23] P. Kočovský, G. Ahmed, J. Šrogl, A.V. Malkov, J. Steele, J. Org. Chem. 64 (1999) 2765.
[24] M. Fuentes, J. Magraner, C. de las Pozas, R. Roque-Malherbe, J. Pérez Pariente, A. Corma, Appl. Catal. 47 (1989) 367.
[25] G.K. Chuah, S.H. Liu, S. Jaenicke, L.J. Harrison, J. Catal. 200 (2001) 352.
[26] K.A. da Silva, P.A. Robles-Dutenhefner, E.M.B. Sousa, E.F. Kozhevnikova, I.V. Kozhevnikov, E.V. Gusevskaya, Catal. Commun. 5 (2004) 425.
[27] Z. Yongzhong, N. Yuntong, S. Jaenicke, G.K. Chuah, J. Catal. 229 (2005) 404.
[28] C. Milone, C. Gangemi, G. Neri, A. Pistone, S. Galvagno, Appl. Catal. A Gen. 199 (2000) 239.
[29] N. Ravasio, N. Poli, R. Psaro, F. Zaccheria, Top. Catal. 13 (2000) 195.
[30] P. Mertens, F. Verpoort, A.N. Parvulescu, D. De Vos, J. Catal. 243 (2006) 7.
[31] P. Mäki-Arvela, N. Kumar, D. Kubicka, A. Nasir, T. Heikkilä, V.P. Lehto, R. Sjöholm, T. Salmi, D.Yu. Murzin, J. Mol. Catal. A Chem. 240 (2005) 72.
[32] K.J. Edler, J.W. White, Chem. Mater. 9 (1997) 1226.
[33] M.J.L. Ginés, C.R. Apesteguía, in: J.J. Spivey, E. Iglesia, T.H. Fleisch (Eds.), Studies in Surface Science and Catalysis, vol. 136, Elsevier, Amsterdam, 2001, p. 447.
[34] P. Grandvallet, P. Courty, E. Freund, A. Sugier, in: Proceedings of the 8th International Congress on Catalysis, Berlin, 1984, vol. II, Ottawa, 1984, pp. 92–99.
[35] A.J. Marchi, J.I. Di Cosimo, C.R. Apesteguía, Catal. Today 15 (1992) 383.
[36] A. Goguet, D. Schweich, J.P. Candy, J. Catal. 220 (2003) 280.
[37] M.K. Oudenhuijzen, P.J. Kooyman, B. Tappel, J.A. van Bokhoven, D.C. Koningsberger, J. Catal. 205 (2002) 135.
[38] I.M.J. Vilella, S.R. de Miguel, C. Salinas-Martinez de Lecea, A. Linares-Solano, O.A. Scelza, Appl. Catal. A Gen. 281 (2005) 247.
[39] J. Court, F. Janati-Idrissi, S. Vidal, in: M. Guisnet, J. Barrault, C. Bouchoule, D. Duprez, G. Pérot, R. Maurel, C. Montassier (Eds.), Studies in Surface Science and Catalysis, vol. 59, Elsevier, Amsterdam, 1991, p. 193.
[40] P. Mäki-Arvela, L.P. Tiainen, M. Lindblad, K. Demirkan, N. Kumar, R. Sjöholm, T. Ollonqvist, J. Väyrynen, T. Salmi, D.Yu. Murzin, Appl. Catal. A Gen. 241 (2002) 271.
[41] F. Delbecq, P. Sautet, J. Catal. 152 (1995) 217.
[42] F. Delbecq, P. Sautet, Catal. Lett. 28 (1994) 89.
[43] P.A. Jacobs, R. von Ballmoos, J. Phys. Chem. 86 (1982) 3050.
[44] M.T. Aronson, R.J. Gorte, W.E. Farneth, J. Catal. 105 (1987) 455.
[45] Ch. Yang, Q. Xu, Zeolites 19 (1997) 404.
[46] A. Vimont, F. Thibault-Starzyk, J.C. Lavalley, J. Phys. Chem. B 104 (2000) 286.
[47] C. Jia, P. Massiani, D. Barthomeuf, J. Chem. Soc. Faraday Trans. 89 (1993) 3659.
[48] J.A. Lercher, Ch. Gründlig, G. Eder-Mirth, Catal. Today 27 (1996) 353.
[49] A. Boreave, A. Aroux, C. Guimon, Micropor. Mater. 11 (1997) 275.
[50] E.P. Parry, J. Catal. 2 (1963) 371.
[51] J.W. Ward, J. Catal. 10 (1968) 34.
[52] H. Knözinger, Adv. Catal. 25 (1976) 184.
[53] J. Wang, L. Huang, H. Chen, Q. Li, Catal. Lett. 55 (1998) 157.
[54] A. Sakthivel, S.E. Dapurkar, N.M. Gupta, S.K. Kulshreshtha, P. Selvam, Micropor. Mesopor. Mater. 65 (2003) 177.
[55] G. Busca, Catal. Today 41 (1998) 191.
[56] G.I. Woolery, G.H. Kuehl, H.C. Timken, A.W. Chester, J.C. Vartuli, Zeolites 19 (1997) 288.
[57] P. Mäki-Arvela, N. Kumar, V. Nieminen, R. Sjöholm, T. Salmi, D.Yu. Murzin, J. Catal. 225 (2004) 155.
[58] N. Ravasio, M. Antenori, F. Babudri, M. Gargano, Stud. Surf. Sci. Catal. 108 (1997) 625.
[59] C. Milone, A. Perri, A. Pistone, G. Neri, S. Galvagno, Appl. Catal. A Gen. 233 (2002) 151.